OncoTargets and Therapy

Dovepress
Taylor & Francis Group

Open Access Full Text Article

ORIGINAL RESEARCH

Coumarins from *Citrus aurantiifolia* (Christm.) Swingle Peel with Potential Cytotoxic Activity Against MCF-7 Breast Cancer Cell Line: In Vitro and In Silico Studies

Euis Julaeha[1], Faryanti Eka Mulyawan[1], Feby Marlia Anwar[1], Abd Wahid Rizaldi Akili[1], Nandang Permadi[2], Darwati[1], Dikdik Kurnia[1], Tati Herlina[1]

[1]Department of Chemistry, Faculty of Mathematics and Natural Sciences, Universitas Padjadjaran, Jatinangor, West Java, 45363, Indonesia; [2]Doctorate Program in Biotechnology, Graduate School, Universitas Padjadjaran, Bandung, West Java, 40132, Indonesia

Correspondence: Euis Julaeha, Email euis.julaeha@unpad.ac.id

Aim: Breast cancer remains a prevalent and challenging health issue for women globally. In the pursuit of more effective and less harmful therapies, researchers have focused on natural compounds, especially phenolic compounds found in various plants and fruits.

Purpose: This study aims to explore the potency of coumarin compounds from *Citrus aurantiifolia* (Christm.) Swingle peel as alternative treatment for breast cancer through in vitro and in silico studies.

Methods: Three coumarins were isolated from *C. aurantiifolia* peel through multiple steps of column chromatograph. Their cytotoxic activities against the MCF-7 breast cancer cell line were evaluated using the MTT assay. Additionally, in silico studies, including molecular docking and molecular dynamics simulations, were conducted to evaluate the interactions of the most potent compound with estrogen receptor alpha (ERα).

Results: Chemical investigation of *C. aurantiifolia* peel led to the isolation of three compounds: 5-geranyloxy-7-methoxycoumarin (1), 5-geranyloxypsoralen (2), and 8-geranyloxypsoralen (3). Cytotoxic assays revealed that compound 2 exhibited the highest cytotoxic potency against MCF-7 breast cancer cell line with an IC_{50} of 138.51 ± 14.44 µg/mL, followed by compounds 1 and 3 with IC_{50} values of 204.69 ± 22.91 and 478.15 ± 34.85 µg/mL, respectively. Molecular docking studies against estrogen receptor alpha (ERα) showed that 5-geranyloxypsoralen (2) had a lower docking score (-10.63 kcal/mol) compared to estradiol (-9.99 kcal/mol). Molecular dynamics simulation revealed the binding stability ERα–Compound 2 complex as evidence from the root mean square deviation (RMSD) of 2.964 ± 0.460 Å. Furthermore, pharmacokinetic predictions suggested that 5-geranyloxypsoralen may possess favourable pharmacokinetic properties, highlighting its potential as a therapeutic agent.

Conclusion: The study highlights the potential of coumarin compounds from *C. aurantiifolia* peel as an alternative treatment for breast cancer, particularly 5-geranyloxypsoralen could be a promising therapeutic agent in breast cancer treatment, warranting further investigation.

Keywords: *C. aurantiifolia*, coumarin compounds, MCF-7, breast cancer, molecular docking

Introduction

Breast cancer remains one of the most prevalent and daunting health challenges facing women worldwide.[1] Characterized by the uncontrolled growth of cells within the breast tissue, this disease can spread to other parts of the body, posing a severe threat to life.[2] Traditional treatments, including surgery, chemotherapy, and radiation, are often accompanied by significant side effects and limitations.[3] In the quest for more effective and less harmful therapies, researchers have turned their attention to natural compounds found abundantly in various plants and fruits.[4]

Coumarins are a class of naturally occurring compounds found in a variety of plants,[5] these compounds are characterized by their benzopyrone structure[6] and are known for their wide range of biological activities, including anti-

Received: 26 November 2024
Accepted: 19 March 2025
Published: 30 March 2025

inflammatory, anticoagulant, antibacterial, antifungal, antiviral, and anticancer properties.[7] Their versatility and potential therapeutic applications have made them a focal point of studies aimed at developing new treatments for various diseases. Among their many effects, the anticancer properties of coumarins have been particularly noteworthy.

Plant species of genus *Citrus* are known as natural sources of coumarins.[8–10] A wide range of secondary metabolites isolated from genus *Citrus* have been evaluated for their potency to fight against cancer cells. Among these natural compounds, coumarins stand out as potential candidates with potent anti-cancer activities. For example, auraptene, imperatorin, phellopterin, and myrsellin isolated from *C. trifoliata* were reported to exhibit significant anti-proliferative against the human colorectal adenocarcinoma tumor cell line.[11,12] On another study, umbelliprenin and auraptene exhibited anti-proliferative effect against cervical cancer cell line, and breast cancer cell line.[13] As our continuous effort to explore the anticancer potency of natural compounds from *Citrus*, in this paper we report the isolation of three coumarins from lime (*C. aurantiifolia*) peel along with their potency as anticancer against MCF-7 breast cancer cell line through both in vitro and in silico studies.

Material and Methods

Sample Preparation

The fruits of *C. aurantiifolia* were obtained from Curah Jati Village, Purwoharjo District, Banyuwangi Regency, East Java, Indonesia. The specimens were verified and documented at the Herbarium Jatinangoriense, Department of Biology, Faculty of Mathematics and Natural Sciences, Universitas Padjadjaran, under the collection reference number 45/HB/02/2021, and identified by Joko Kusmoro. Prior to solvent extraction, the peel of *C. aurantiifolia* was separated from the fruit and distilled using hydrodistillation at 100°C to isolate the essential oil for other research purposes. Subsequently, the peel was dried in the oven at 40°C and then ground into powder.

The secondary metabolites from the *C. aurantiifolia* peel residues were extracted through successive maceration technique. Briefly, a total of 2 kg of *C. aurantiifolia* peel powder was soaked with n-hexane at room temperature. During the maceration process, the samples were manually agitated using glass rode every 24 hours. After four days of maceration, the n-hexane filtrate was collected and concentrated using a rotary evaporator at approximately 40°C. On the other hand, the remaining powder residue underwent maceration with ethyl acetate, following the same procedure. The ethyl acetate filtrate was evaporated under vacuo, yielding 23.45 g of concentrated ethyl acetate extract.

Coumarin Compounds Isolation

A total of 23 g of ethyl acetate extract was separated using vacuum liquid chromatography (VLC) on a GF254 silica gel stationary phase. The dimensions of the VLC column used were 15 cm in height and 5 cm in diameter. The eluents used were n-hexane, ethyl acetate, and methanol, added in a gradient with a 10% increase in polarity. Fractions with similar thin layer chromatography (TLC) spot patterns were combined, concentrated, and further separated. Fraction B (5.0018 g) was separated using a G60 silica gel stationary phase (0.063–0.200 mm) with n-hexane:ethyl acetate (9:1) as the eluent. Fraction B1 (105.8 mg) was then separated using the same stationary phase with n-hexane:methylene chloride: ethyl acetate (7:2:1) as the eluent, yielding compound 1 (73.1 mg). Meanwhile, fraction B2 (405.2 mg) was separated using ethyl acetate:n-hexane:methylene chloride:ethyl acetate (6:2:2) as the eluent, yielding compound 2 (114.5 mg).

Fraction C (1.2 g) was separated using open column chromatography with a gradient of n-hexane:ethyl acetate (5%), resulting in seven combined fractions labeled C1-C7. Fraction C4 (102.9 mg) was further separated using open column chromatography with a gradient of n-hexane:ethyl acetate (1%), yielding six combined fractions labeled C4A-C4F. Fraction C4C (69.2 mg) was then subjected to another round of open column chromatography using n-hexane:methylene chloride (4:6) as the eluent, which led to the isolation of compound 3 as a white solid (34.8 mg).

Chemical Structure Determination

The structures of compounds 1–3 were determined by analyzing data from ultraviolet (UV) spectroscopy, infrared spectroscopy (IR), mass spectrometry (MS), proton nuclear magnetic resonance spectroscopy (^{1}H-NMR), and carbon nuclear magnetic resonance spectroscopy (^{13}C-NMR). The UV spectrum of compound 1–3 was recorded using a UV-

1800 Shimadzu spectrophotometer. The IR spectrum was recorded using a One Perkin Elmer Spectrum FTIR spectrometer, whereas the mass spectrum was recorded using a Waters Xevo QTOF spectrometer, and the NMR spectrum was recorded using a JEOL ECZ-500 spectrometer at 500 MHz. The NMR spectrum of compound 1–3 was analyzed using delta 6.0.0 software.

In Vitro Cytotoxic Assay

MCF-7 cells (ATCC HTB-22) were cultured in RPMI-1640 medium supplemented with 10% Fetal Bovine Serum (FBS) and 50 µL/50 mL antibiotics. The cells were incubated in 96-well plates for 24 hours at 37°C and 5% CO_2. Subsequently, samples of varying concentrations were added to the plates. The concentration variations were achieved by dissolving the samples in DMSO. In this assay, DMSO was used as the negative control (solvent), while cisplatin was used as the positive control. After 24 hours of incubation, 10% PrestoBlue reagent was added to each well, and the incubation was continued for 1 hour until a color change was observed. SDS stopper was then added, and the absorbance was measured at λ=570 nm using a multimode reader. The IC_{50} value was determined from a graph of the percentage of viable cells compared to the control (%), which contained only FBS and DMSO, against the sample concentration (µg/mL).

Molecular Docking and Molecular Dynamics Simulation

In this study, the human estrogen receptor alpha (ERα) ligand–binding domain was used for molecular docking and molecular dynamics simulation. The 3D X-ray crystal structure of the protein was retrieved from the Protein Data Bank (PDB) (https://www.rscb.org, accessed on 27 October 2024) with PDB ID of 3ERT. The protein was downloaded as a complex of ERα with 4-hydroxytamoxifen as the co-crystallized ligand.[14]

Before performing molecular docking for the compound of interest, a redocking procedure was carried out to validate the molecular docking protocol. The Biovia Discovery Studio (DS) 2021 Client software was used to remove water from the protein-ligand complex. Following, the protein and ligand were separated and individually saved as pdb files. Both of the protein and ligand files were further processed using AutoDockTools 1.5.6. and each was saved as pdbqt format file. The redocking procedure was performed using AutoDock4 (v4.2.6). The grid box size was set to 40 × 40 × 40 with center coordinates of 31.349, −1.602, and 25.604 (x, y, z) and a spacing of 0.375 Å. The redocking procedure yielded a root mean square deviation (RMSD) of 1.02 Å, indicating that the molecular docking procedure was valid.[15] The AutoDock4 scoring function was used to calculate the binding energy of the docked configuration.[16]

The protonation state of the compound of interest at physiological pH of 7.4 was predicted using Chemaxon MarvinSketch software. The three-dimensional (3D) structure was then generated and optimized using the MMFF94 force field with Avogadro software and saved in the pdb format. This 3D structure was processed for molecular docking using AutoDockTools 1.5.6. and saved in the pdbqt format. Subsequently, the structure underwent molecular docking, adhering to the protocol outlined for the redocking process.

The molecular dynamics (MD) simulation was performed using the Particle-Mesh Ewald Molecular Dynamics (PMEMD) module within AMBER20, with GPU acceleration as described in our previous study.[17] The initial minimization process included 1000 steps using the steepest descent method followed by 2000 steps of the conjugate gradient method, applying a harmonic force of 5 kcal mol^{-1} $Å^{-2}$. This was succeeded by 5000 steps of unrestricted conjugate gradient minimization to rectify any spatial overlaps. The system's temperature was progressively increased to 300 K in 20 ps increments (0-100 K, 100-200 K, and 200-300 K), taking a total of 60 ps. An equilibration phase followed, ensuring stable density, pressure, and gradual force release over 1000 ps. Finally, production runs were conducted for 100 ns, with each step lasting 2 fs.[18] The ccptraj program within AmberTools21 was utilized to carry out the MD trajectory analyses, which included RMSD and root mean square fluctuation (RMSF). Additionally, the ante-MMPBSA.py in AmberTools21 was utilized for the calculation of the MMGBSA binding energy and energy decomposition analysis of the protein-ligand complex.

In silico Toxicity and Pharmacokinetics Prediction

The toxicity and pharmacokinetics of compound 2 were predicted using the ADMETlab 2.0 web server (https://admetmesh.scbdd.com/ accessed October 27th, 2024) as described in our previous study.[19]

Results

Structure Elucidation of Compound 1-3

Compound 1 was obtained as white needle-like crystal. The UV spectrum of compound 1 in methanol solvent showed the presence of four peaks. The absorption at λ_{max} 227 nm (ε 6.699) and 251 nm (ε 13.289) indicates the presence of electronic transition of α,β-unsaturated system from the K band. Additionally, the presence of weak absorption at λ_{max} 313 nm from the R band and 268 nm of the B band indicates the presence of aromatic system in the chemical structure of compound 1. The IR spectrum showed the presence of C=O functional group (V_{max} = 1735 cm^{-1}), aromatic C=C (1614 cm^{-1}), geminal dimethyl (1440 and 1364 cm^{-1}), C-H sp^2 (3091 cm^{-1}), C-H sp^3 (2969 and 2912 cm^{-1}), and C-O bond (1158 cm^{-1}). The HR-TOFMS spectrum revealed that compound 1 has *m/z* of 329.1747 $[M+H]^+$ (calculated 329.1753 for $C_{20}H_{25}O_4^+$). ^{1}H-NMR (500 MHz, acetone-D6) δ_H (ppm): 1.56 (3H, *s*, H-9'), 1.61 (3H, *s*, H-10'), 1.75 (3H, s, H-4'), 2.12 (2H, *m*, H-5' dan H-6'), 3.87 (3H, *s*, O-CH_3), 4.69 (2H, *d, J* = 6.5 Hz, H-2'), 5.09 (1H, *m*, H-7'), 5.49 (1H, *td, J* = 6.5; 1.0 Hz, H-2'), 6.09 (1H, *d*, 9.5, H-3), 6.43 (1H, *s*, H-3), 6.45 (1H, *s*, H-8), and 7.99 (1H, *d*, 9.5, H-4). ^{13}C-NMR (125 MHz, acetone-D6) δ_C (ppm): 15.9 (C-4'), 16.9 (C-9'), 24.9 (C-10'), 26.1 (C-6'), 39.3 (C-5'), 55.5 (C-7), 65.7 (C-1'), 92.8 (C-8), 95.7 (C-10), 103.7 (C-6), 110.7 (C-6), 119.1 (C-2'), 123.8 (C-7'), 131.3 (C-8'), 138.5 (C-4), 141.5 (C-5), 156.4 (C-5), 156.9 (C-9), 160.2 (C-7), and 164 (C-2). The NMR spectrum of compound 1 is consistent with 5-geranyloxy-7-methoxycoumarin reported in the literature.[20]

Compound 2 was obtained as yellow oil. UV (MeOH) λ_{max}: 225 (ε 8.207), 252 (ε 11.588), 312 (ε 923), and 269 (ε 9.536) nm. HRTOF-MS: *m/z* 339.1580 $[M+H]^+$ (calculated 339.1596, $C_{21}H_{23}O_4^+$). ^{1}H-NMR (500 MHz, acetone-D6) δ_H (ppm): 1.57 (3H, *brs*, H-9'); 1.63 (3H, *brs*, H-10'); 1.67 (3H, *brs*, H-4'); 2.07 (2H, *m*, H-5' and H-6'); 5.03 (2H, *d*, 7.1); 5.04 (1H, *s*, H-7'); 6.27 (1H, *d, J*= 9.8 Hz); 7.15 (1H, *dd, J*= 2.5; 1.0 Hz); 7.18 (1H, *brs*); 7.15 (1H, *dd, J*= 2.5; 1.0 Hz); and 7.78 (1H, *d, J*=2.4 Hz). ^{13}C-NMR (125 MHz, acetone-D6) δ_C (ppm): 16.7 (C-10'), 17.7 (C-9'), 25.7 (C-8'), 26.2 (C-5'), 39.5 (C-4'), 69.8 (C-1'), 94.2 (C-8), 105.1 (C-6), 107.5 (C-10), 112.5 (C-3), 114.2 (C-11), 118.9 (C-2'), 123.5 (C-6'), 132 (C-7'), 123.5 (C-6'), 132 (C-7'), 139.7 (C-4), 143.1 (C-3'), 144.9 (C-7), 149 (C-5), 152.7 (C-9), 158.1 (C-12), 161.3 (C-2). The NMR spectrum of compound 2 is consistent with 5-geranyloxypsoralen reported in the literature.[20]

Compound 3 was obtained as white solid. UV (MeOH) λ_{max}: 248 nm (ε 17.211), 218 nm (ε 17.583), 301 nm (ε 91). IR (KBr pellets) V_{max} cm^{-1}: 2923 (C-H), 1819 (C=O), 1586 (C=C). HRTOF-MS: *m/z* 361.1429 $[M+Na]^+$ (calculated 361.1416, $C_{21}H_{22}O_4Na^+$). ^{1}H NMR (500 MHz, $CDCl_3$): 1.54 (3H, *s*); 1.62 (3H, *s*); 1.67 (3H, *s*); 1.98 (4H, *d, J* = 2.5 Hz); 4.97 (1H, *m*); 5.01 (2H, *d, J* = *7* Hz); 5.56 (1H, *t, J* = *7* Hz and 14 Hz), 6.34 (1H, *d, J* = 9.5 Hz); 6.79 (1H, *d, J* = 2.5 Hz); 7.34 (1H, *s*); 7.67 (1H, *d, J* = 2.5 Hz); 7.74 (1H, *d, J* = 9.5 Hz). ^{13}C NMR (125 MHz, $CDCl_3$): 16.6 (C-10"); 17.7 (C-9"); 25.7 (C-8"); 26.4 (C-5"); 39.6 (C-4"); 70.1 (C-1"); 106.8 (C-3'); 113.3 (C-5); 114.7 (C-3); 116.5 (C-10); 119.4 (C-2"); 123.8 (C-6"); 125.9 (C-6); 131.6 (C-8); 131.8 (C-7"); 143.2 (C-9); 144.0 (C-3"); 144.4 (C-4); 146.7 (C-2"); 148.8 (C-7); 160.6 (C-2). The NMR spectrum of compound 3 is consistent with 8-geranyloxypsoralen reported in the literature.[21]

Cytotoxic Activity of Compound 1-3 Against MCF-7 Breast Cancer Cell Line

The cytotoxic activity against MCF-7 breast cancer cell line of the ethyl acetate extract of *C. aurantiifolia* peel, compound 1-3 were evaluated using the resazurin assay (Table 1). According to the United States National Cancer Institute (USNCI), the cytotoxic activity of a compound is classified as highly cytotoxic if the IC_{50} value is <20 μg/mL, moderate if the IC_{50} is between 21 and 200 μg/mL, weak if the IC_{50} is between 201 and 500 μg/mL, and non-cytotoxic if the IC_{50} is >500 μg/mL.[22]

The cytotoxic assay revealed that the ethyl acetate fraction of *C. aurantiifolia* peel exhibited stronger inhibitory activity against the MCF-7 breast cancer cell line compared to compounds 1-3. This enhanced activity may be attributed to the synergistic effects of multiple chemical compounds present in the ethyl acetate fraction.[23] Among the isolated compounds, 5-geranyloxy psoralen (2) showed better cytotoxic activity compared to 5-geranyloxy-7-methoxycoumarin (1) and 8-geranyloxypsoralen (3).

Table 1 Cytotoxic activity of *C. aurantiifolia* ethyl acetate extract and compound 1–3 against MCF-7 breast cancer cell line

Sample	IC_{50}		Category
	µg/mL	µM	
Ethyl acetate extract	69.34 ± 0.85	–	Moderate
5-geranyloxy-7-methoxycoumarin (1)	204.69 ± 22.91	623.27 ± 67.9	Weak
5-geranyloxypsoralen (2)	138.51 ± 14.44	409.31 ± 45.3	Moderate
8-geranyloxypsoralen (3)	478.15 ± 34.85	1412.98 ± 102.98	Weak
Cisplatin	3.99 ± 0.08	13.22 ± 0.28	Highly toxic

Molecular Docking and Molecular Dynamics Simulation of Compound 2 Against ERα

The cytotoxic assay against the MCF-7 breast cancer cell line revealed that compound 2 exhibited the highest inhibitory activity among all the compounds being evaluated. Given this promising result, the next step involved conducting molecular docking studies against ERα. Molecular docking studies revealed that compound 2 binds to ERα with a docking score of -10.63 kcal/mol. While this docking score is slightly higher (less negative) than that of the standard drug, 4-hydroxytamoxifen (-12.26 kcal/mol), it is more favorable than that of estrogen (-9.99 kcal/mol), which is the substrate of ERα (Table 2). The RMSD plot of ERα apoenzyme and ERα–compound 2 complex derived from a 100 ns molecular dynamics simulation is given in Figure 1. The RMSD value of ERα–compound 2 complex was 2.964 ± 0.460 Å, whereas the apo form was 2.302 ± 0.307 Å. The RMSF analysis for each amino acid residues of ERα are represented in Figure 2.

In Silico ADMET Prediction of Compound 2

The toxicity prediction suggested that compound 2 demonstrates a relatively favorable safety profile with some concerns. It is predicted to exhibit a low risk of hERG blockers, indicating a minimal likelihood of interfering with cardiac ion channels that could lead to heart arrhythmias. Additionally, compound 2 shows a low risk of being mutagenic or carcinogenic, suggesting it is unlikely to cause genetic mutations or contribute to cancer development. However, compound 2 does present a medium risk of drug-induced liver injury and high risk of human hepatotoxicity, indicating potential for liver damage when used at certain dosages or over extended periods. The pharmacokinetic predictions of compound 2, including its absorption, distribution, metabolism, and excretion (ADME) properties, are presented in Table 3.

Table 2 Docking scores of compound 2, 4-hydroxytamoxifen, and estrogen–ERα complexes derived from molecular docking

Compound	Docking Score (kcal/mol)	Interaction with Amino Acid Residues	
		Hydrogen Bond	Hydrophobic
4-Hydroxytamoxifen	-12.26	Arg394, Glu353	**Pi-Alkil**: Leu525, Met421, Met388, Ile424, Leu428, Leu391, Leu387. **Pi-Pi Stacked**: Leu346 **Pi-Sulfur**: Met343
Estradiol	-9.99	His524, Arg394	**Pi-Alkil**: Ile424, Leu384, Leu387, Met388, Ala350, Leu391, Leu525, Leu346 **Pi-Pi T-Shaped**: Phe404
5-Geranyloxy psoralen	-10.63	Arg394	**Pi-Alkil**: Leu428, His524, Leu525, Leu346, Leu384, Ala350, Leu387, Trp383 **Pi-Sigma**: Leu391 **Pi-Pi Stacked**: Phe404 **Pi-Sulfur**: Met421, Met388

https://doi.org/10.2147/OTT.S506978

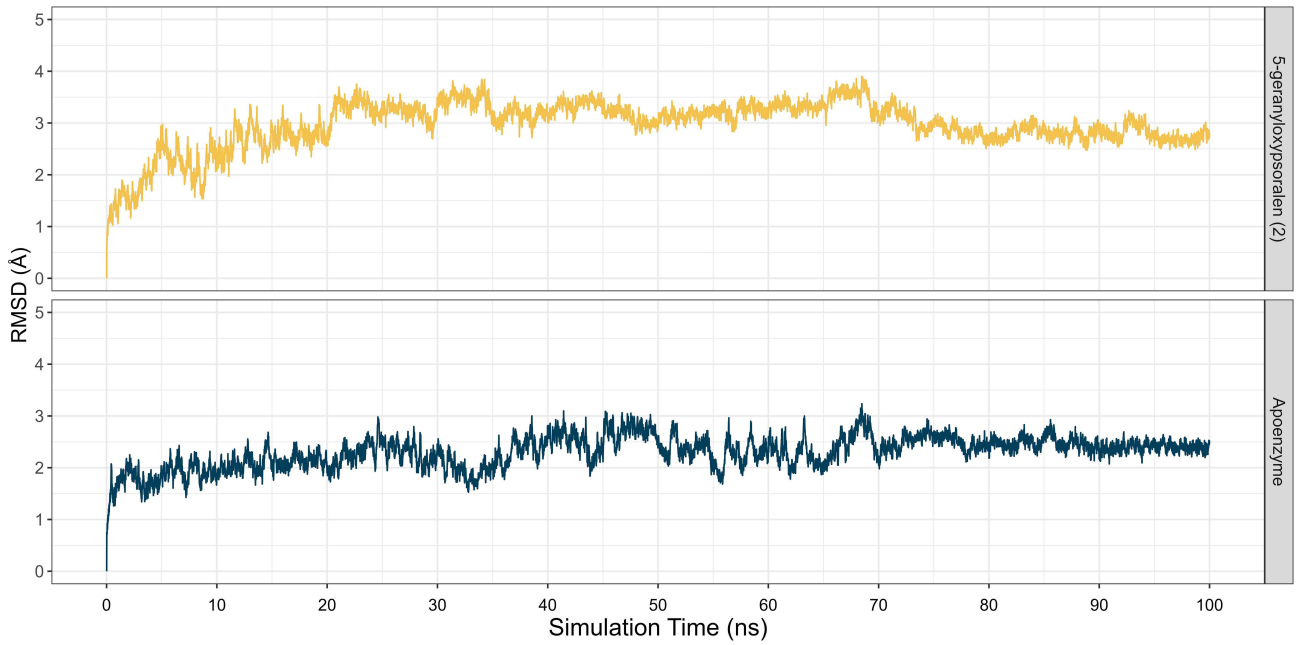

Figure 1 The RMSD plot of ERα apoenzyme and ERα–compound 2 complex over 100 ns time trajectory.

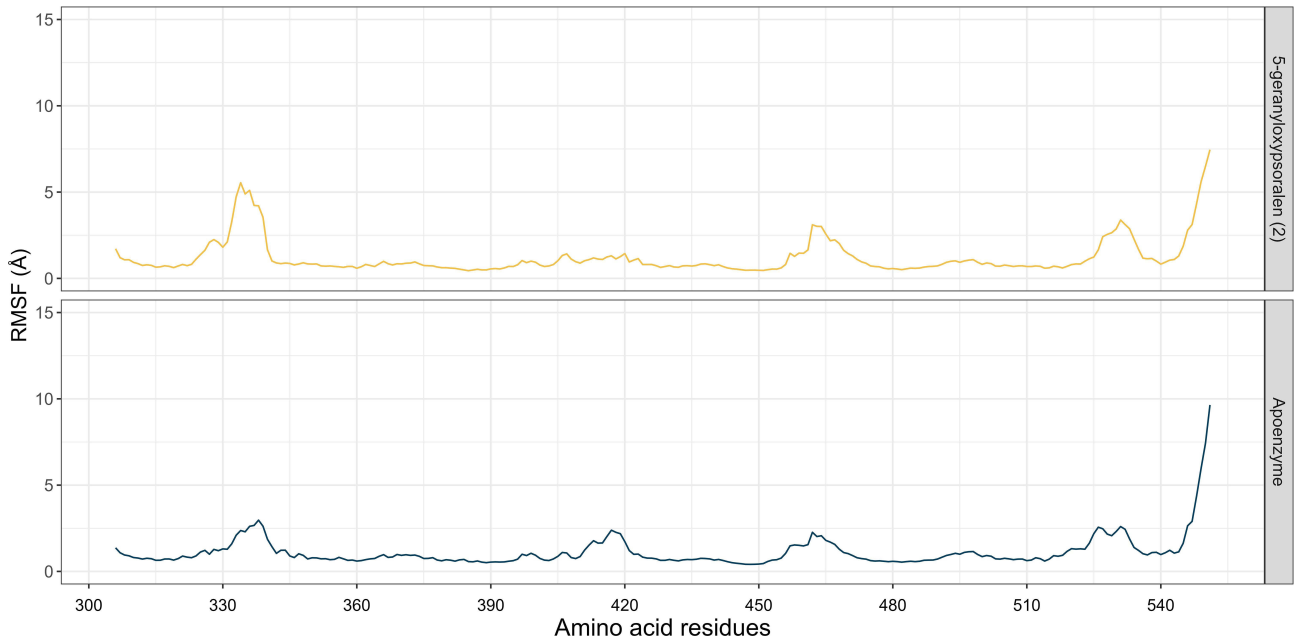

Figure 2 The RMSF plot of ERα apoenzyme and ERα–compound 2 complex over 100 ns time trajectory.

Discussion

In this study, we investigated the potential cytotoxic activity of coumarin compounds isolated from the peel of *C. aurantiifolia* against the MCF-7 breast cancer cell line. Chemical investigation of the ethyl acetate fraction of *C. aurantiifolia* has led to the isolation of three coumarin compounds. The chemical structures of these coumarin compounds were determined through multiple spectroscopy methods and were identified as 5-geranyloxy-7-methoxy-coumarin (1), 5-geranyloxypsoralen (2), 8-geranyloxypsoralen (3) (Figure 3).

Table 3 Pharmacokinetics prediction of compound 2

Pharmacokinetic Property	Parameters	Predicted Values
Absorption	Caco-2 permeability	-4.776 log cm/s
	MCDK Permeability	1.9 x 10^{-5} cm/s
	Pgp-Inhibitor	No
	Pgp-Substrate	No
	Human Intestinal Absorption	High
Distribution	Protein Binding	91.648%
	Volume distribution	1.028
	Blood Brain Barrier Penetration	Yes
	Fraction unbound	8.809%
Metabolism	CYP1A2 inhibitor	Yes
	CYP1A2 substrate	No
	CYP2C19 inhibitor	Yes
	CYP2C19 substrate	No
	CYP2C9 inhibitor	Yes
	CYP2C9 substrate	Yes
	CYP2D6 inhibitor	Yes
	CYP2D6 substrate	Yes
	CYP3A4 inhibitor	Yes
	CYP3A4 substrate	No
Excretion	Clearance	10.8 mL/min/kg
	Half-life	0.116

The cytotoxicity of compound 1-3 along with the ethyl acetate fraction was evaluated against MCF-7 breast cancer cell line. The result revealed that the ethyl acetate fraction of *C. aurantiifolia* peel exhibited stronger inhibitory activity compared to compounds 1-3. This enhanced activity may be attributed to the synergistic effects of multiple chemical compounds present in the ethyl acetate fraction.[23] Among the isolated compounds, 5-geranyloxy psoralen (2) showed better cytotoxic activity compared to 5-geranyloxy-7-methoxycoumarin (1) and 8-geranyloxypsoralen (3). Although our research does not report the cytotoxicity of compound 2 on normal cells, Zhang et al, (2019) reported that compound 2 did not exhibit cytotoxic effects on normal cells.[24]

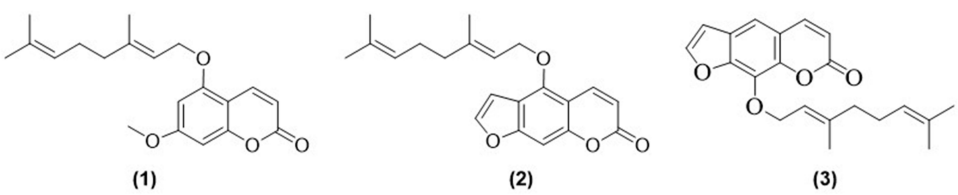

Figure 3 Chemical structure of compound 1-3.

https://doi.org/10.2147/OTT.S506978

Analysis of the chemical structures of compounds 1-3 and their corresponding cytotoxic activities highlights the crucial role of the geranyloxy position in determining cytotoxic efficacy. Both compounds 1 and 2, which have the geranyloxy group at the C5 position, exhibited higher cytotoxic effects compared to compound 3, which has the geranyloxy group at the C8 position. This suggests that the position of the geranyloxy group is critical for enhancing cytotoxic activity against MCF-7 cells. The important role of the geranyloxy group at the C5 position to enhance cytotoxic activity of coumarins is supported by a previous study, which showed that 5-geranyloxycoumarin exhibited enhanced cytotoxic effect against HeLa cell line compared to 3-geranyloxycoumarin, 4-geranyloxycoumarin, and 7-geranyloxycoumarin.[25]

In the development and progression of the MCF-7 breast cancer cell line, ERα plays a pivotal role to trigger a series of signaling pathways that promote cell proliferation, survival, and differentiation.[26] MCF-7 cells are ERα-positive, meaning they express high levels of this receptor, which is activated by the hormone estrogen.[27] The cytotoxic assay against the MCF-7 breast cancer cell line revealed that compound 2 exhibited the highest inhibitory activity among all the compounds being evaluated. Given this promising result, the next step involved conducting molecular docking studies against ERα. Molecular docking studies revealed that despite the docking score of compound 2 is slightly higher (less negative) than that of the standard drug, 4-hydroxytamoxifen, it is more favorable than that of estrogen, which is the substrate of ERα.

Figure 4 illustrates the molecular interaction comparison between 4-hydroxytamoxifen and compound 2 within the ligand-binding pocket of ERα. Both 4-hydroxytamoxifen and compound 2 establish hydrogen bonds with Arg394, a critical amino acid residue essential for binding estrogen. Arg394 interacts with the phenolic hydroxyl moiety of estrogen, underscoring its importance in maintaining receptor-ligand stability.[28] Additionally, both compounds engage with hydrophobic residues, including Leu525, Leu346, and Met421. These interactions contribute significantly to the binding affinity and stability of the complexes, especially Leu346 is considered as antiestrogenic residue which plays a crucial role in the recognition of antiestrogenic ligands.[29,30] Furthermore, both compounds exhibit π-π stacking interactions with Met343, further enhancing their binding within the receptor's pocket.

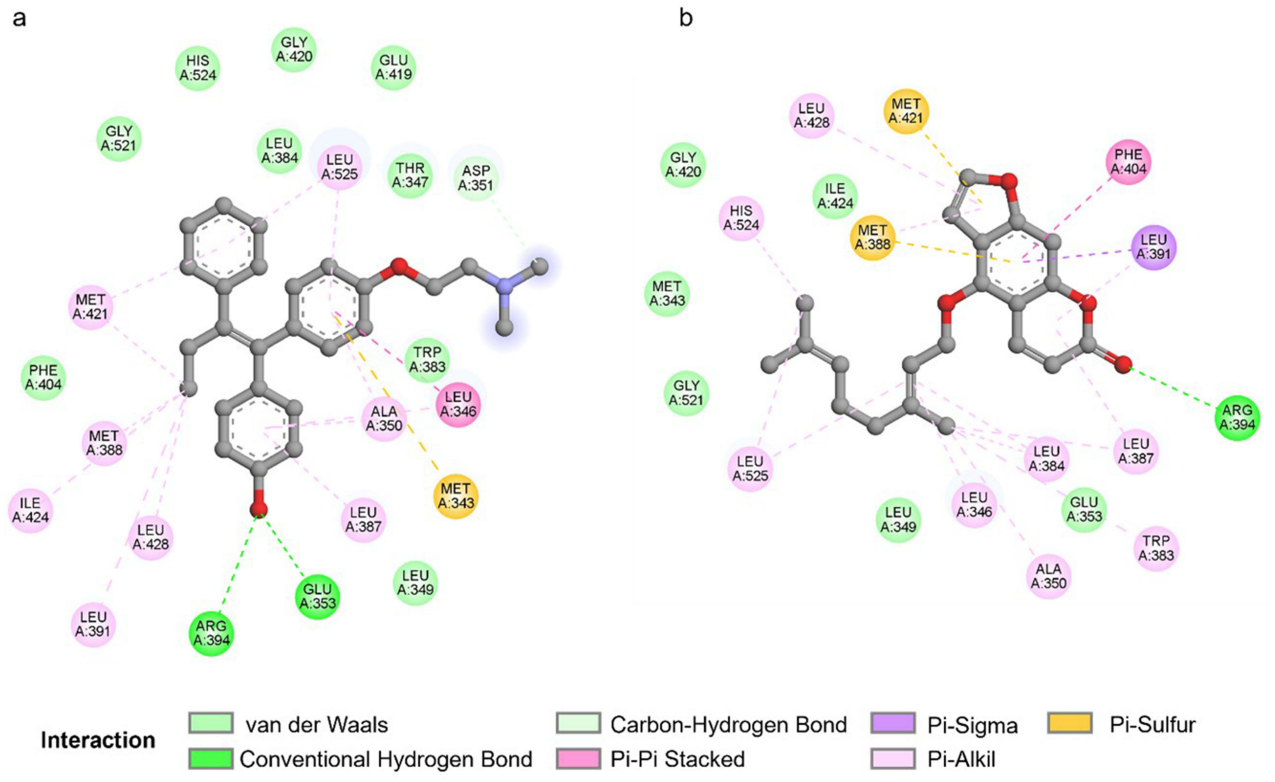

Figure 4 Molecular interaction of 4-hydroxytamoxifen (**a**) and compound 2 (**b**) within the ligand binding pocket of ERα.

In addition to molecular docking, molecular dynamics simulation was conducted to further evaluate the stability of ERα–compound 2 complex and the complex-free binding energy. In molecular dynamics simulation, the RMSD values could be employed to analyze the stability of protein-ligand complex.[31] The 100 ns molecular dynamics simulation revealed that there is conformational change in the Apo form of ERα as the binding effect of compound 2. Though the ERα–compound 2 complex exhibited higher RMSD than that of the Apo form of ERα, the complex is considered stable since the RMSD value does not exceed 3 Å.[32] The conformational change of ERα–compound 2 complex is further supported by the RMSF plot (Figure 2). RMSF analysis revealed that several amino acids underwent significant fluctuation, these are including Asp332 (3.28 Å), Pro333 (4.73 Å), Thr334 (5.54 Å), Arg335 (4.89), Pro336 (5.09 Å), Phe337 (4.23 Å), Ser338 (4.20 Å), Lys531 (3.38 Å), Asn532 (3.12 Å), His547 (3.12 Å), Arg548 (4.32 Å), Leu549 (5.59 Å), His550 (6.49 Å), and Ala551 (7.46 Å). Furthermore, the MMGBSA free binding energy calculation revealed the binding energy of ERα–compound 2 complex was -46.36 ± 2.56 kcal/mol. The amino acid residues that responsible for molecular recognition of compound 2 are represented in Figure 5. From the MMGBSA free energy decomposition analysis, revealed that among these amino acid residues, Ala350 (-3.18 ± 0.64 kcal/mol); Glu 353 (-0.92 ± 0.30 kcal/mol); Arg394 (-1.73 ± 0.44 kcal/mol), Leu387 (-4.43 ± 0.48 kcal/mol), Leu391 (-2.63 ± 0.18 kcal/mol), Leu525 (-2.58 ± 0.21 kcal/mol), Met343 (-1.30 ± 0.27 kcal/mol), Met388 (-2.63 ± 0.19 kcal/mol), Met343 are also present in the binding of OHT, which is the antagonist of ERα. Hydrogen bond analysis (Figure 6) revealed that during the 100 ns simulation, compound 2 generally formed only one hydrogen bond with Arg394, with a fraction of 0.024. This finding further underscores the significance of Arg394 in the binding stability of the ERα–compound 2 complex.

Preliminary toxicity prediction is a critical component of drug discovery and development, as it helps identify potential safety issues early in the process, thereby reducing the risk of costly failures in later stages.[33] In terms of toxicity, compound 2 demonstrates a relatively favorable safety profile with some concerns. It is predicted to exhibit a low risk of hERG blockers, indicating a minimal likelihood of interfering with cardiac ion channels that could lead to heart arrhythmias. Additionally, compound 2 shows a low risk of being mutagenic or carcinogenic, suggesting it is unlikely to cause genetic mutations or contribute to cancer development. However, compound 2 does present a medium risk of drug-induced liver injury and high risk of human hepatotoxicity, indicating potential for liver damage when used at certain dosages or over extended periods. Nevertheless, according to Yazici et al, (2023), compound 2 does not induce hepatotoxicity; rather, it exhibits hepatoprotective properties. Compound 2 was reported to prevent paracetamol-induced

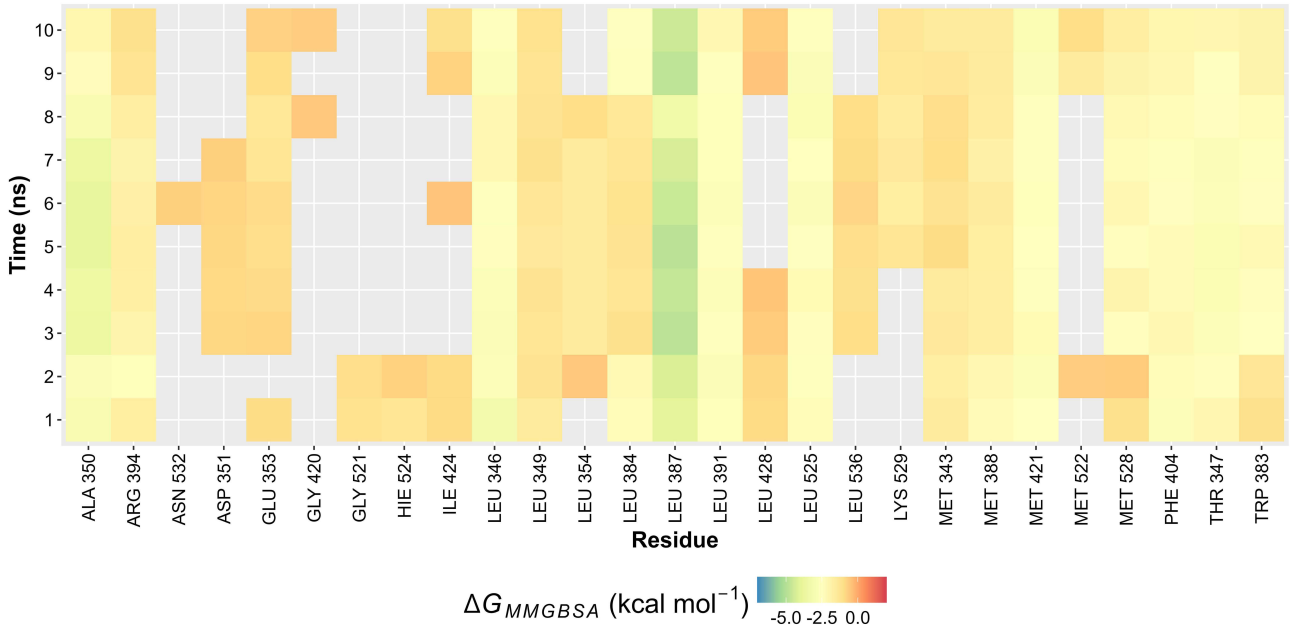

Figure 5 Heatmap representation of MMGBSA binding energy decomposition for amino acid residues of ERα ligand binding pocket that interact with compound 2.

https://doi.org/10.2147/OTT.S506978

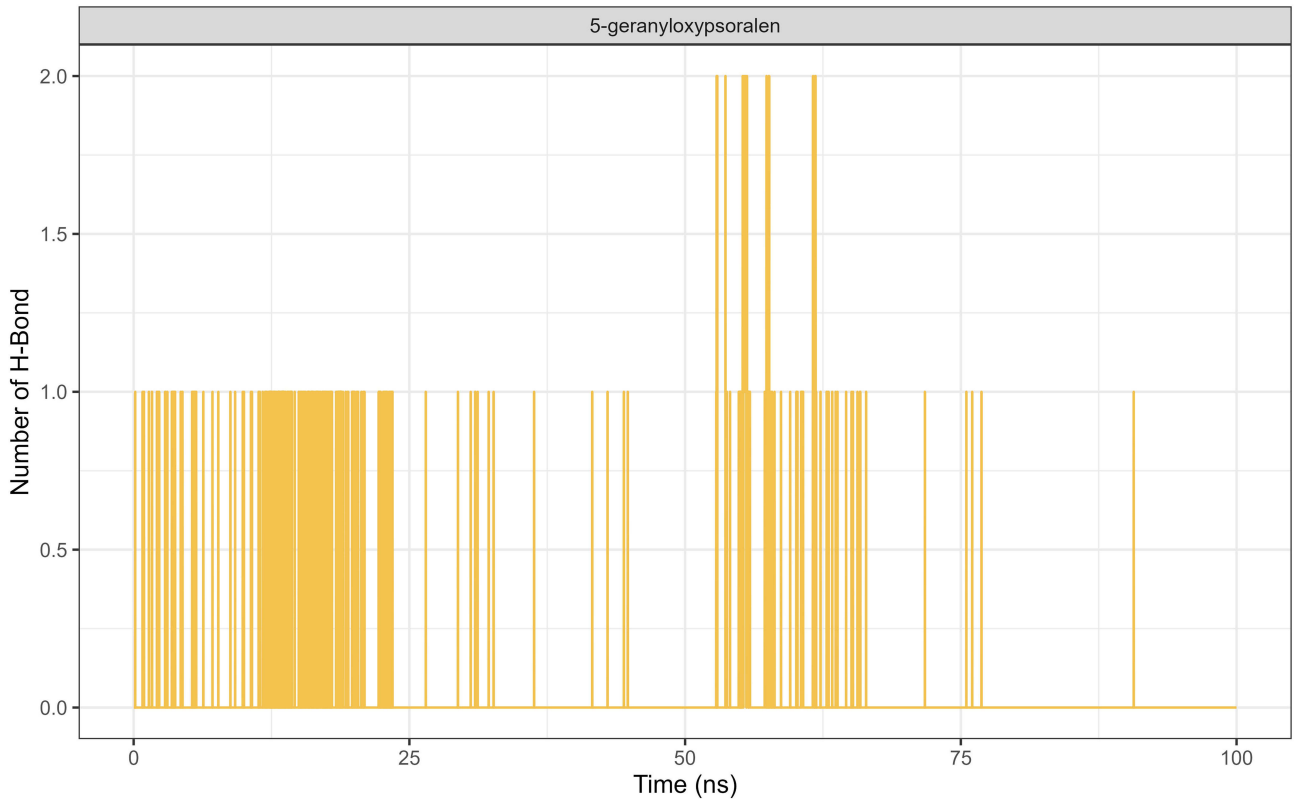

Figure 6 Hydrogen bond analysis of ERα–compound 2 complex from 100 ns molecular dynamics trajectories.

hepatotoxicity in rats after an overdose, demonstrating its potential to protect the liver from acute damage caused by hepatotoxic agents.[34]

In addition to toxicity prediction, pharmacokinetics prediction is also important as it provides early insights into a drug candidate's ADME properties. The pharmacokinetics prediction of compound 2 is given in Table 3. In terms of drug absorption, compound 2 is predicted to have high permeability in both Caco-2 and MDCK cell lines, suggesting efficient absorption through the intestinal epithelium and a good potential for bioavailability. Furthermore, compound 2 is identified as a poor P-glycoprotein (Pgp) inhibitor and is not a substrate of Pgp. This indicates a reduced likelihood of being actively effluxed out of cells by Pgp transporters, which often limits the absorption and distribution of many drugs. Additionally, the high human intestinal absorption further supports its potential for effective oral administration.

In terms of drug distribution, compound 2 exhibits several favourable pharmacokinetic properties. It shows high protein plasma binding, indicating that a significant portion of the drug binds to plasma proteins, potentially prolonging its circulation time in the bloodstream. The compound also displays an appropriate volume of distribution, suggesting it is well distributed throughout bodily tissues. Additionally, compound 2 demonstrates high blood–brain barrier (BBB) penetration, crucial for targeting central nervous system (CNS) disorders such as Alzheimer's Disease. Moreover, it has a medium fraction unbound, indicating a balanced proportion of the drug remains free in the plasma to exert its therapeutic effects.

Regarding metabolism, compound 2 is predicted to undergo modification by the cytochrome P450 enzymes CYP2D6 and CYP2C9. These enzymes play a crucial role in the metabolism of many drugs, suggesting compound 2 may be metabolized efficiently in the liver. Additionally, compound 2 has the potential to inhibit the activity of several CYP enzymes, including CYP1A2, CYP2C19, CYP2C9, CYP2D6, and CYP3A4. This broad inhibition profile could have significant implications for drug interactions, affecting the metabolism of other co-administered drugs that are substrates for these enzymes. The inhibition of these enzymes could lead to increased plasma concentrations of other drugs, potentially causing adverse effects or toxicity. Therefore, careful consideration of

drug–drug interactions and dose adjustments may be necessary when compound 2 is used in combination with other medications.

Though compound 2 exhibited high value of IC_{50}, which potentially rise challenges in achieving therapeutic concentrations of compound 2 in vivo. Despite this hurdle, compound 2 shows promising therapeutic potential. Advanced drug delivery systems, such as nanoparticle-based carriers or liposomes, can be utilized to enhance the bioavailability and targeted delivery of compound 2, ensuring higher local concentrations at the site of action.[35,36] Additionally, using compound 2 in combination with other agents that have synergistic effects may lower the required therapeutic dose and enhance overall efficacy. By implementing these strategies, the limitations posed by the high IC_{50} values of compound 2 can be mitigated, thereby enhancing its translational potential for therapeutic applications.

Conclusion

Chemical investigation of *C. aurantiifolia* peel resulted in the isolation of three compounds: 5-geranyloxy-7-methoxycoumarin (1), 5-geranyloxypsoralen (2), and 8-geranyloxypsoralen (3). Cytotoxic assays revealed that compound 2 exhibited the highest cytotoxic potency against MCF-7 breast cancer cell line, with an IC_{50} of 138.51 ± 14.44 µg/mL, followed by compounds 1 and 3 with IC_{50} values of 204.69 ± 22.91 µg/mL and 478.15 ± 34.85 µg/mL, respectively. The structure–activity relationship analysis highlighted the critical role of the geranyloxy group's position in enhancing the cytotoxic activity of these compounds against MCF-7 breast cancer cell line. Molecular docking study against ERα showed that 5-geranyloxypsoralen (2) exhibited lower docking score compared to estrogen. Furthermore, molecular dynamics simulation revealed the stable-binding ERα–compound 2 as evidence from RMSD values. In addition, toxicity and pharmacokinetics predictions revealed that compound 2 possesses a relatively favorable toxicity and pharmacokinetics profile, further supporting its promise as a candidate for further preclinical evaluation and development. These findings highlight the therapeutic potential of compound 2 and emphasize the importance of structural modifications in optimizing cytotoxic efficacy.

Acknowledgments

The authors are grateful to Universitas Padjadjaran for providing funds through the Academic Leadership Grant (ALG) scheme (No.5417/UN6.3.1/PT.00/2024) by Euis Julaeha.

Disclosure

The authors report no conflicts of interest in this work.

References

1. Arnold M, Morgan E, Rumgay H, et al. Current and future burden of breast cancer: global statistics for 2020 and 2040. *Breast*. 2022;61:66. doi:10.1016/j.breast.2022.08.010
2. Lukong KE. Understanding breast cancer – the long and winding road. *BBA Clin*. 2017;7:64–77. doi:10.1016/j.bbacli.2017.01.001
3. Debela DT, Muzazu SGY, Heraro KD, et al. New approaches and procedures for cancer treatment: current perspectives. *SAGE Open Med*. 2021:9. doi:10.1177/20503121211034366.
4. Bakrim S, El Omari N, El Hachlafi N, et al. Dietary phenolic compounds as anticancer natural drugs: recent update on molecular mechanisms and clinical trials. *Foods*. 2022;11(21). doi:10.3390/foods11213323
5. Anywar G, Muhumuza E. Bioactivity and toxicity of coumarins from African medicinal plants. *Front Pharmacol*. 2023;14. doi:10.3389/fphar.2023.1231006
6. Heghes SC, Vostinaru O, Mogosan C, et al. Safety profile of nutraceuticals rich in coumarins: an update. *Front Pharmacol*. 2022:13. doi:10.3389/fphar.2022.803338.
7. Annunziata F, Pinna C, Dallavalle S, et al. An overview of coumarin as a versatile and readily accessible scaffold with broad-ranging biological activities. *Int J Mol Sci*. 2020;21(13). doi:10.3390/ijms21134618
8. Sanches VL, Cunha TA, Viganó J, et al. Comprehensive analysis of phenolics compounds in citrus fruits peels by UPLC-PDA and UPLC-Q/TOF MS using a fused-core column. *Food Chem X*. 2022;14:100262. doi:10.1016/j.fochx.2022.100262
9. Nurzaman M, Permadi N, Setiawati T, et al. DPPH free radical scavenging activity of *Citrus aurantifolia* Swingle peel extracts and their impact in inhibiting the browning of *Musa paradisiaca* L. var. Kepok Tanjung explants. *Jordan J Biol Sci*. 2022;15(5). doi:10.54319/jjbs/150505
10. Kaur S, Singh V, Chopra HK, et al. Extraction and characterization of phenolic compounds from mandarin peels using conventional and green techniques: a comparative study. *Discover Food*. 2024;4(1):60. doi:10.1007/s44187-024-00139-y
11. Kerekes D, Horváth A, Kúsz N, et al. Coumarins, furocoumarins and limonoids of *Citrus trifoliata* and their effects on human colon adenocarcinoma cell lines. *Heliyon*. 2022;8(9):e10453. doi:10.1016/j.heliyon.2022.e10453

12. Wu CP, Murakami M, Li YC, et al. Imperatorin restores chemosensitivity of multidrug-resistant cancer cells by antagonizing ABCG2-mediated drug transport. *Pharmaceuticals*. 2023;16(11):1595. doi:10.3390/ph16111595
13. Wang H, Liu Y, Wang Y, et al. Umbelliprenin induces autophagy and apoptosis while inhibits cancer cell stemness in pancreatic cancer cells. *Cancer Med*. 2023;12(14):15277–15288. doi:10.1002/cam4.6170
14. Shiau AK, Barstad D, Loria PM, et al. The structural basis of estrogen receptor/coactivator recognition and the antagonism of this interaction by tamoxifen. *Cell*. 1998;95(7):927–937. doi:10.1016/S0092-8674(00)81717-1
15. AbdWR A, Hardianto A, Latip J, et al. Virtual screening and ADMET prediction to uncover the potency of flavonoids from genus *Erythrina* as antibacterial agent through inhibition of bacterial ATPase DNA gyrase B. *Molecules*. 2023;28(24):8010. doi:10.3390/molecules28248010
16. Hill AD, Reilly PJ. Scoring functions for autodock. *Meth Mol Biol*. 2015;1273. doi:10.1007/978-1-4939-2343-4_27
17. Herlina T, Akili AWR, Nishinarizki V, et al. Cytotoxic evaluation, molecular docking, molecular dynamics, and ADMET prediction of isolupalbigenin isolated from *Erythrina subumbrans* (Hassk). Merr. (Fabaceae) stem bark: unveiling its anticancer efficacy. *Onco Targets Ther*. 2024;17:829–840. doi:10.2147/OTT.S482469
18. Hardianto A, Mardetia SS, Destiarani W, et al. Unveiling the anti-cancer potential of onoceranoid triterpenes from *Lansium domesticum* Corr. cv. kokosan: an in silico study against estrogen receptor alpha. *Int J Mol Sci*. 2023;24(19). doi:10.3390/ijms241915033
19. Akili AWR, Thurfah NA, Hardianto A, et al. Investigating the potency of *Erythrina*–derived flavonoids as cholinesterase inhibitors and free radical scavengers through in silico approach: implications for Alzheimer's disease therapy. *Adv Appl Bioinfo Chem*. 2024;17:107–118. doi:10.2147/AABC.S483115
20. Sandoval-Montemayor NE, García A, Elizondo-Treviño E, et al. Chemical composition of hexane extract of *Citrus aurantifolia* and anti-*Mycobacterium tuberculosis* activity of some of its constituents. *Molecules*. 2012;17(9):11173–11184. doi:10.3390/molecules170911173
21. Wang XB, Li GH, Li L, et al. Nematicidal coumarins from *Heracleum candicans* Wall. *Nat Prod Res*. 2008;22(8):666–671. doi:10.1080/14786410701766463
22. Sajjadi SE, Ghanadian M, Haghighi M, et al. Cytotoxic effect of *Cousinia verbascifolia* Bunge against OVCAR-3 and HT-29 cancer cells. *J HerbMed Pharmacol*. 2015;4(1):15–19.
23. Nordin ML, Abdul Kadir A, Zakaria ZA, et al. In vitro investigation of cytotoxic and antioxidative activities of *Ardisia crispa* against breast cancer cell lines, MCF-7 and MDA-MB-231. *BMC Complement Altern Med*. 2018;18(1). doi:10.1186/s12906-018-2153-5
24. Zhang H, Yang ST, Lin T. Bergamottin exerts anticancer effects on human colon cancer cells via induction of apoptosis, G2/M cell cycle arrest and deactivation of the Ras/Raf/ERK signalling pathway. *Arch Med Sci*. 2022;18(6). doi:10.5114/aoms.2019.86226
25. Maleki EH, Bahrami AR, Sadeghian H, et al. Discovering the structure–activity relationships of different O-prenylated coumarin derivatives as effective anticancer agents in human cervical cancer cells. *Toxicol in Vitro*. 2020:63. doi:10.1016/j.tiv.2019.104745.
26. Liao XH, Lu DL, Wang N, et al. Estrogen receptor α mediates proliferation of breast cancer MCF –7 cells via a p21/ PCNA / E 2 F 1-dependent pathway. *FEBS J*. 2014;281(3):927–942. doi:10.1111/febs.12658
27. Porras L, Ismail H, Mader S. Positive regulation of estrogen receptor alpha in breast tumorigenesis. *Cells*. 2021;10(11):2966. doi:10.3390/cells10112966
28. McCullough C, Neumann TS, Gone JR, et al. Probing the human estrogen receptor-α binding requirements for phenolic mono- and di-hydroxyl compounds: a combined synthesis, binding and docking study. *Bioorg Med Chem*. 2014;22(1):303–310. doi:10.1016/j.bmc.2013.11.024
29. Li WM, Li XB, Sun SX, et al. Agonist and antagonist recognition studies for oestrogen receptor by molecular dynamics simulation. *Mol Simul*. 2013;39(3):228–233. doi:10.1080/08927022.2012.717281
30. Sinyani A, Idowu K, Shunmugam L, et al. A molecular dynamics perspective into estrogen receptor inhibition by selective flavonoids as alternative therapeutic options. *J Biomol Struct Dyn*. 2023;41(9):4093–4105. doi:10.1080/07391102.2022.2062786
31. Aier I, Varadwaj PK, Raj U. Structural insights into conformational stability of both wild-type and mutant EZH2 receptor. *Sci Rep*. 2016;6(1):34984. doi:10.1038/srep34984
32. Padhi AK, Janežič M, Zhang KYJ. Molecular dynamics simulations: principles, methods, and applications in protein conformational dynamics. *Adv Protein Mol Struct Biol Meth*. 2022;2022:439–454. doi:10.1016/B978-0-323-90264-9.00026-X
33. Uesawa Y. Efficiency of pharmaceutical toxicity prediction in computational toxicology. *Toxicol Res*. 2024;40(1):1–9. doi:10.1007/s43188-023-00215-y
34. Yazıcı E, Şahin E, Alvuroğlu E, et al. Bergamottin reduces liver damage by suppressing inflammation, endoplasmic reticulum and oxidative stress in cafeteria diet-fed mice. *Food Biosci*. 2023:52. doi:10.1016/j.fbio.2023.102371.
35. Mall J, Naseem N, MdF H, et al. Nanostructured lipid carriers as a drug delivery system: a comprehensive review with therapeutic applications. *Intelligent Pharm*. 2024;2024:1. doi:10.1016/j.ipha.2024.09.005
36. Ashfaq R, Rasul A, Asghar S, et al. Lipid nanoparticles: an effective tool to improve the bioavailability of nutraceuticals. *Int J Mol Sci*. 2023;24(21). doi:10.3390/ijms242115764